Psychiatry Research: Neuroimaging 301 (2020) 111107

Contents lists available at ScienceDirect

Psychiatry Research: Neuroimaging

journal homepage: www.elsevier.com/locate/psychresns

Effects of sex, age, and apolipoprotein E genotype on hippocampal parenchymal fraction in cognitively normal older adults

Babak A. Ardekani[*,a,b], Neema O. Izadi[a], Somar A. Hadid[a], Amir M. Meftah[a], Alvin H. Bachman[a], for the Alzheimer's Disease Neuroimaging Initiative[1]

[a] Center for Brain Imaging and Neuromodulation, The Nathan S. Kline Institute for Psychiatric Research, Orangeburg, NY, USA
[b] Department of Psychiatry, New York University School of Medicine, New York, NY, USA

ARTICLE INFO

Keywords:
Brain
MRI
Hippocampus
Atrophy
Healthy aging
Apolipoprotein E ϵ4
Sex
Alzheimer's disease
Mild cognitive impairment
Hippocampal parenchymal fraction
Neurodegeneration
Hippocampal volumetric integrity

ABSTRACT

Early detection of Alzheimer's disease (AD) is important for timely interventions and developing new treatments. Hippocampus atrophy is an early biomarker of AD. The hippocampal parenchymal fraction (HPF) is a promising measure of hippocampal structural integrity computed from structural MRI. It is important to characterize the dependence of HPF on covariates such as age and sex in the *normal* population to enhance its utility as a disease biomarker. We measured the HPF in 4239 structural MRI scans from 340 cognitively normal (CN) subjects aged 59-89 years from the AD Neuroimaging Initiative database, and studied its dependence on age, sex, apolipoprotein E (*APOE*) genotype, brain hemisphere, intracranial volume (ICV), and education using a linear mixed-effects model. In this CN cohort, HPF was inversely associated with ICV; was greater on the right hemisphere compared to left in both sexes with the degree of right > left asymmetry being slightly more pronounced in men; declined quadratically with age and faster in *APOE* ϵ4 carriers compared to non-carriers; and was significantly associated with cognitive ability. Consideration of HPF as an AD biomarker should be in conjunction with other subject attributes that are shown in this research to influence HPF levels in CN older individuals.

1. Introduction

Hippocampus (HC) atrophy is a well-established imaging predictor of incipient Alzheimer's disease (AD) in patients with mild cognitive impairment (MCI) (Jack et al., 1999). Recently, a multi-center study conducted in 17 European memory clinics showed that, in patients under clinical evaluation for cognitive impairment, addition of quantitative bilateral HC volumetry to the traditional diagnostic workup had a measurable impact on the diagnostic confidence of AD pathology (Bosco et al., 2017).

The most direct method for characterizing HC atrophy on MRI is by manually tracing its boundary on high-resolution structural MRI scans using specialized software (Convit et al., 1997; Jack et al., 1998; Konrad et al., 2009; Nestor et al., 2013). Unfortunately, manual measurement is tedious, requires extensive operator training, and tracing protocols vary significantly across laboratories. Added to these difficulties are findings of possible visual perceptive bias whereby estimated volumes depend on the orientation of the image as presented to a human rater (Maltbie et al., 2012; Rogers et al., 2012). These issues all but rule out using manual measurement of HC volume as a viable approach to routine clinical assessment of HC structural integrity.

While excellent progress has been made towards development of automated MRI-based algorithms for HC segmentation (Cardoso et al., 2013; Chupin et al., 2009; Collins and Pruessner, 2010; Coupe et al., 2010; 2011; Dill et al., 2015; Fischl et al., 2002; Hu et al., 2011; Morra et al., 2008; Nestor et al., 2013; Zhou and Rajapakse, 2005), these methods are less robust compared to manual measurements (Mulder et al., 2014), can be computationally expensive (Fischl et al., 2002), and often require extensive preprocessing of the MRI scans (inhomogeneity correction, distortion correction, etc.) and technical operator expertise (Morra et al., 2008).

Early in the development of neuroimaging biomarkers of HC atrophy in AD, de Leon et al. (1993) recognized the value of examining the accumulation of cerebrospinal fluid (CSF) in the perihippocampal

* Corresponding author at: Center for Brain Imaging and Neuromodulation, The Nathan S. Kline Institute for Psychiatric Research, 140 Old Orangeburg Road, Orangeburg, NY 10962, USA. Tel.: +1 845 398 5490.
E-mail address: ardekani@nki.rfmh.org (B.A. Ardekani).

[1] Data used in preparation of this article were obtained from the Alzheimer's Disease NeuroimagingInitiative (ADNI) database (adni.loni.usc.edu). As such, the investigators within the ADNI contributed tothe design and implementation of ADNI and/or provided data but did not participate in analysis or writingof this report. A complete listing of ADNI investigators can be found at: http://adni.loni.usc.edu/wp-content/uploads/how to apply/ADNI Acknowledgement List.pdf.

https://doi.org/10.1016/j.pscychresns.2020.111107
Received 13 January 2020; Received in revised form 24 March 2020; Accepted 15 April 2020
Available online 14 May 2020
0925-4927/

fissures along the axis of the HC formation in CT scans as an indication of volume loss. Using similar ideas, an alternative approach to characterizing HC atrophy has been to formulate variables that can be measured from MRI scans which in some sense reflect compromised HC structural integrity, but are not direct measurements of HC volume per se (Heister et al., 2011; Lee et al., 2019; Rusinek et al., 2003; Suppa et al., 2015). The basic premise behind this group of techniques is that neurodegeneration tends to replace brain parenchyma with CSF. Hence the measurements in some sense try to capture the relative volume, and change thereof, between brain parenchyma and CSF in well-defined regions of interest in the medial temporal lobe.

Following this approach, the hippocampal parenchymal fraction (HPF) is a recently developed structural MRI biomarker of the HC volumetric integrity. It has been shown to be a sensitive marker of compromised HC in AD (Ardekani et al., 2016), mild cognitive impairment (MCI) (Ardekani et al., 2017; Mubeen et al., 2017), first-episode psychosis (Goff et al., 2018), mesial temporal lobe epilepsy (Hakimi et al., 2019), and normal cognitive decline in aging (Bruno et al., 2016). HPF is estimated rapidly ($<$ 1 minute per scan), robustly ($<$ 2% failure rate), and requires no preprocessing of the MRI scans. Its computation is fully automatic and does not require operator expertise.

To fully realize the clinical potential of HPF as a neuroimaging biomarker of HC atrophy, it is important to establish its normative values in cognitively healthy aging. To this end, the main objective of this study was to establish normative values of HPF with respect to age, sex, *APOE* genotype, and brain hemisphere in a large cohort of cognitively normal (CN) older adults. Another aim was to determine the association between HPF and cognitive ability. Guided by several recent studies from our group and others, we hypothesized that: (1) HPF will decline with age, (2) there is a right greater than left asymmetry, (3) the asymmetry is greater in men, (4) the rate of decline with age is higher in *APOE* ϵ4 carriers, and (5) HPF explains variations in cognitive ability beyond that explained by sex, age and *APOE* genotype.

2. Materials and methods

2.1. Study subjects

Data used in this study were obtained from the Alzheimer's Disease Neuroimaging Initiative (ADNI) database (adni.loni.usc.edu). The ADNI was launched in 2003 as a public-private partnership, led by Principal Investigator Michael W. Weiner, MD. The primary goal of ADNI has been to test whether serial MRI, positron emission tomography (PET), other biological markers, and clinical and neuropsychological assessment can be combined to measure the progression of MCI and early AD. For up-to-date information, see adni.loni.usc.edu.

Since the main aim of the present study was to obtain normative values for HPF, we selected a cohort of cognitively normal (CN) subjects from ADNI. Briefly, ADNI inclusion criteria for CN subjects included: age between 55-90 (inclusive); absence of memory complaints beyond age expectation; normal memory function documented by scoring above education adjusted cutoffs on the Logical Memory II subscale (Delayed Paragraph Recall, Paragraph A only) from the Wechsler Memory Scale Revised; Mini-Mental State Exam (MMSE) score between 24 and 30 (inclusive); Clinical Dementia Rating (CDR) 0; absence of significant impairment in cognitive functions or activities of daily living; stability of permitted medications for 4 weeks; less than 6 Geriatric Depression Scale; and Hachinski ischemic score less than or equal to 4. Exclusion criteria included: any significant neurologic disease, such as Parkinson's disease, multi-infarct dementia, Huntington's disease, normal pressure hydrocephalus, brain tumor, progressive supranuclear palsy, seizure disorder, subdural hematoma, multiple sclerosis, or history of significant head trauma followed by persistent neurologic defaults or known structural brain abnormalities; major depression, bipolar disorder as described in DSM-IV within the past 1 year; history of schizophrenia; MRI contraindications; history of alcohol or substance abuse or dependence within the past 2 years; residence in skilled nursing facility; and current use of specific psychoactive medications (e.g., certain antidepressants, neuroleptics, chronic anxiolytics or sedative hypnotics, etc.).

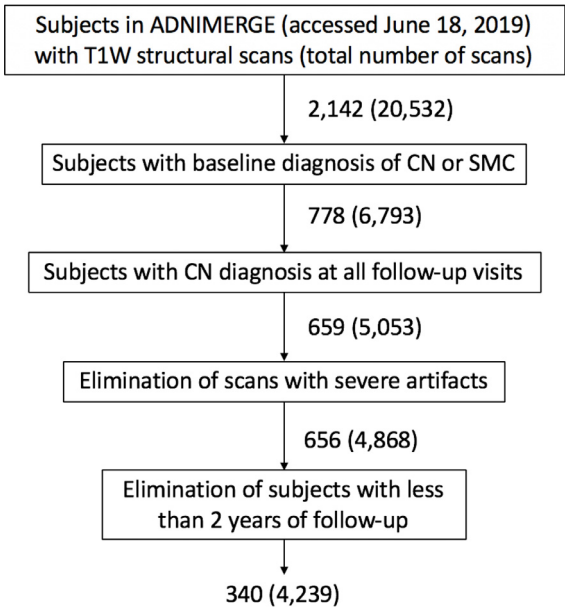

Fig. 1. Cohort selection procedure.

Our method of identifying the cohort used in this study is shown in Figure 1. ADNI datafiles MPRAGEMETA.csv and ADNIMERGE.csv were accessed on June 18, 2019. Using the information in these datafiles, we identified 2,142 subjects with a total of 20,532 three-dimensional (3D) T_1-weighted structural MRI scans. From these, we eliminated all subjects with a baseline diagnosis (DX_bl) other than cognitively normal (CN) or significant memory concern (SMC), reducing the number of subjects to 778 with a total of 6,793 scans. Next, we eliminated all subjects with any follow-up diagonsis (DX) of MCI or AD, reducing the cohort to 659 subjects with 5,053 scans, acquired from September 2005 through April 2019. All scans were downloaded from the ADNI website and visually inspected for artifacts. Consequently, we identified and eliminated 185 scans with various artifacts which included: truncated field-of-view, more than moderate subject motion, excessive noise, severe B_1 field inhomogeneity, scan being other than T_1-weighted, etc. After elinimating these scans, the cohort reduced to 656 subjects with 4,868 scans. Finally, we only retained the subjects who had at least two years duration of observation obtaining our final cohort of 340 subjects with 4,239 scans.

2.2. MRI protocols

The 4239 3D T_1-weighted scans had been acquired at 59 different ADNI MRI centers. The MRI scanners included multiple 1.5 T and 3 T models from three main manufacturers: GE, Philips, and Siemens. The MRI scans were acquired using either MP-RAGE (magnetization prepared rapid gradient echo) or IR-FSPGR (inversion recovery prepared fast spoiled gradient recalled) pulse sequences. The MRI pulse sequences included both fully sampled and accelerated parallel imaging acquisitions (GRAPPA on Siemens and SENSE on Philips and GE). Detailed acquisition parameters for various platforms are available from the ADNI website: http://adni.loni.usc.edu/methods/documents/mri-protocols. Imaging protocols are described in detail by Jack et al. (2015, 2010, 2008).

2.3. ADAS-Cog-13 data

The Alzheimer's Disease Assessment Scale–Cognitive Subscale (ADAS-Cog) consists of a brief cognitive test battery designed to assess the severity of cognitive dysfunction (Rosen et al., 1984). During the examination, subjects are asked to perform 11 specific cognitive and memory tasks that are both written tests and observer-based assessments. These tasks include word recall, constructional and ideational praxis, language, orientation, and comprehension of spoken language. ADAS-Cog-13 adds two additional tasks to this battery: a test of delayed word recall and a number cancellation or maze task (Mohs et al., 1997). ADAS-Cog-13 is scored from 0 to 85 by summing the number of errors made in each task; therefore, a higher score indicates more errors and worse performance. We were able to match 1873 ADAS-Cog-13 assessments to scans within 60 days of scan dates.

2.4. Image processing

Within each subject, scans were aligned using the ATRA module of the Automatic Registration Toolbox (ART). This is a symmetric, unbiased registration technique that computes a rigid-body transformation matrix for each scan such that all scans are registered to a common standardized orientation. ATRA relies on automatic mid-sagittal plane (MSP) detection and automatic detection of the mid-sagittal cross-sectional points of the anterior commissure (AC) and posterior commissure (PC). The MSP is detected using the method described in Ardekani et al. (1997). The AC/PC are detected using the method described in Ardekani and Bachman (2009). In 82 of the 4239 volumes (1.9%), the MSP and/or AC/PC detection failed. ATRA provides a mechanism for the operator to manually supply the MSP and AC/PC, in which case, ATRA bypasses the automated detection steps. Therefore, we were still able to process the 82 cases and obtain HPF values by supplying the MSP and AC/PC manually.

Following intra-subject registration, the KAIBA module of ART was used to compute the left and right HPF. Details of this algorithm have been presented elsewhere (Ardekani et al., 2016; Goff et al., 2018). Briefly, a probabilistic volume-of-interest (PVOI) is projected onto the native space of the 3D structural MRI scan, as shown in Figure 2. The projection is based on a landmark-based 12-parameter affine transformation. We visually inspected the PVOI in all 4239 exams and confirmed that they were projected correctly similar to the case shown in Figure 2.

Once the PVOI is determined, the histogram of all voxels with non-zero probabilities is computed and a Gaussian mixture model (GMM) is fitted to the histogram as shown in Figure 3. The smooth GMM fit allows the algorithm to determine a gray matter peak indicated by I_{gm} on Figure 3. The algorithm also computes a "maximum" intensity value indicated by I_{max} as the 99.75 percentile intensity value. Finally, a CSF intensity threshold (I_{CSF} in Figure 3) is defined as:

$$I_{CSF} = I_{gm} - .2I_{max}$$

The HPF is defined as the ratio of the number voxels with intensities above I_{CSF} threshold to the total number of PVOI voxels with non-zero probabilities. It represents the estimated fraction of the PVOI that is occupied by brain parenchyma as opposed to CSF. HPF varies between 0 and 1. Lower values indicate a greater degree of hippocampal atrophy.

Algorithms that intend to characterize left/right differences in the brain have to ensure that the computed measures are left/right unbiased. Specifically, any computed measure should be invariant with respect to a left/right reflection of the neuroimage. KAIBA ensures that the estimated HPF is unbiased with respect to hemispheric laterality by computing and averaging a pair of HPF values for each hemisphere: once using the original MRI volume and a second time using its mirror reflection with respect to the mid-sagittal plane. The final HPF value for each hemisphere is then given as the average of the two HPF values obtained for that hemisphere.

2.5. Statistical analysis

Statistical analyses were performed using the R statistical computing program version 3.5.2 (R Core Team, 2018). HPF data were analyzed by fitting linear mixed-effects regression models using the lme4 package in R (Bates et al., 2015).

In the first analysis, HPF (HPF_{ijk}) was considered as the dependent variable, and age (A_{ij}), sex (S_j), hemisphere (H_k), *APOE* ϵ4 carrier status ($APOE4_j$), field strength (B_{ij}), intracranial volume (ICV) denoted by V_j, and education level (E_j) were included as fixed effects along with a random intercept (b_j) and a random slope (a_j) for each subject. The precise model fitted is given by:

$$\begin{aligned} HPF_{ijk} \;=\; & \beta_0 + b_j + \beta_1 S_j + \beta_2 H_k + \beta_3 S_j H_k + \beta_4 B_{ij} + \beta_5 \\ & E_j \;+ \\ & \beta_6 APOE4_j + (\beta_7 + a_j + \beta_8 APOE4_j) A_{ij} + \beta_9 \\ & A_{ij}^2 + \beta_{10} V_j + e_{ij} \end{aligned} \tag{1}$$

All terms in model (1) are defined in Table 1. The ICV values (V_j) were downloaded directly from ADNI and converted to z-scores. The model accounts for non-linear dependence of HPF on age by including quadratic age terms A_{ij} and A_{ij}^2, both centered around the subjects median age at the baseline scan (73 years). Hypotheses may be tested by considering specific contrasts of the model parameters $\beta_0 \cdots \beta_{10}$.

In the second analysis, we modeled the ADAS-Cog-13 scores ($ADAS13_{ij}$) in terms of age, sex, education, HPF, and *APOE* ϵ4 carrier status. Since the left and right HPF are highly correlated, in this analysis, we used their average across hemispheres. Also, if multiple scans were associated with a single ADAS-Cog-13 assessment, we averaged the HPF across these scans. The precise statistical model for this

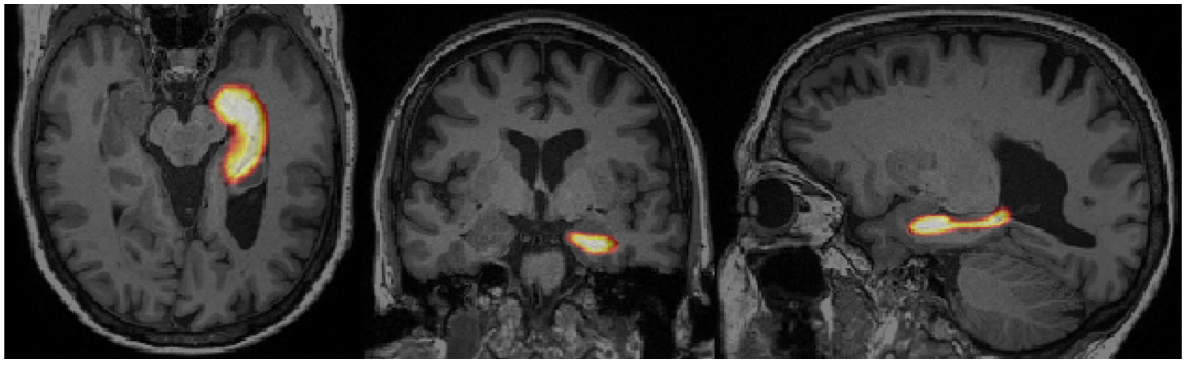

Fig. 2. The probabilistic volume of interest (PVOI) for the left hippocampus is shown as a semi-transparent overlay in "hot" colormap on axial (left), coronal (middle) and sagittal (right) sections through a 3D structural MRI scan in native space.

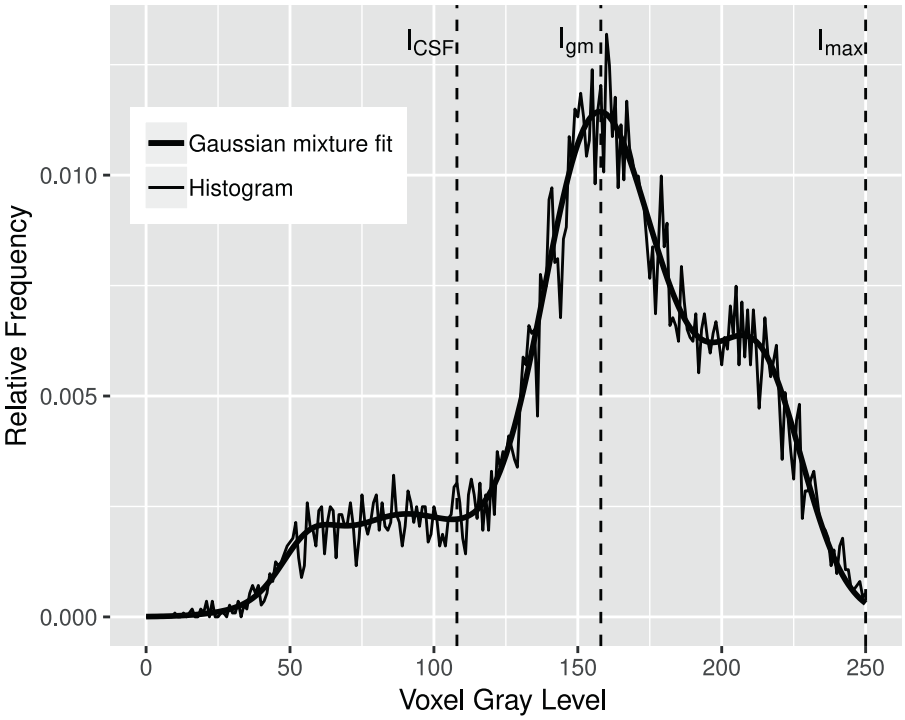

Fig. 3. The normalized histogram of the voxel intensities comprising the hippocampus PVOI in Figure 2 is shown (thin jagged line) along with a 5-component Gaussian mixture model fit (thick smooth line). Smooth fitting allows us to estimate the gray matter peak location I_{gm} (indicated by the dashed line at intensity 158) and 99.75 percentile intensity I_{max} (indicated by the dashed line at intensity 250) from which we determine the location of a CSF intensity threshold I_{CSF} (indicated by the dashed line at intensity 108) as $I_{CSF} = I_{gm} - .2I_{max}$. HPF is defined as the area under the histogram for intensities above I_{CSF}.

Table 1
Mathematical notation in statistical model (1)

k	Hemisphere index $k = l$ for left, $k = r$ for right
j	Subject index $j = 1, 2, \ldots, 340$
n_j	Number of scans from jth subject
i	Scan index $i = 1, 2, \ldots, n_j$
HPF_{ijk}	HPF measured on scan i, subject j, and hemisphere k
A_{ij}	Centered age (actual minus 73)
APOE4_j	*APOE* ϵ4 carrier status (carrier = 1, non-carrier = 0)
B_{ij}	Scanner field strength (3 T= 0, 1.5 T= 1)
E_j	Centered years of education (actual minus 16)
H_k	Hemisphere indicator ($H_r = 1$, $H_l = 0$)
S_j	Sex (male = 1, female = 0)
V_j	Standardized ICV
b_j	Random intercept for jth subject; $b_j \sim N(0, \sigma_b^2)$
a_j	Random slope for jth subject; $a_j \sim N(0, \sigma_a^2)$
$\beta_0 \cdots \beta_{10}$	Model parameters
e_{ij}	Random residual; $e_{ij} \sim N(0, \sigma_e^2)$

Table 2
Subject demographics

	Total	Male	Female	*P*-value
Number of subjects	340	162 (47.6%)	178 (52.4%)	.39
Baseline age (yrs)	73.64 (5.84)	74.14 (6.25)	73.18 (5.43)	.13
APOE ϵ4 (+, -)	87, 253	38, 124	49, 129	.39
Years of education (yrs)	16.5 (2.7)	17.1 (2.3)	15.9 (2.8)	< .001
ICV (cm^3)	1511 (154.5)	1602 (139.3)	1429 (116.8)	< .001
Number of 3 T scans	2502 (59%)	1179 (56.2%)	1323 (61.8%)	< .001
Number of 1.5 T scans	1737 (41%)	920 (43.8%)	817 (38.2%)	″

Numbers in parentheses are standard deviations or percentages as applicable.

analysis is given by:

$$\begin{aligned}\text{ADAS13}_{ij} \;=\; & \beta_0 + b_j + \beta_1 \text{APOE4}_j + \beta_2 S_j + \beta_3 \\ & \text{HPF}_{ij} \times 100 + \\ & \beta_4 E_j + (\beta_5 + a_j + \beta_6 \text{APOE4}_j) A_{ij} + \beta_7 \\ & A_{ij}^2 + e_{ij}. \end{aligned} \tag{2}$$

Definitions of the mathematical notation in model (2) are similar to those in model (1) given in Table 1.

3. Results

The actual P values are reported unless $P < .001$. When estimates are reported as percentages, they are with respect to .861, the mean HPF marginalized across sexes and hemispheres for a hypothetical *APOE* ϵ4 non-carrier subject with median age (73 yrs), median education level (16 yrs), and mean ICV (1511 cm^3), scanned at 3 T. Quoted estimates are followed by either their standard deviation or 95% confidence interval in parenthesis.

3.1. Sample characteristics

Demographic characteristics of the subjects are shown in Table 2. The sample was balanced with respect to sex ($\chi^2 = .75$, $df = 1$, $P = .39$), consisting of 162 men (47.6%) and 178 women (52.4%). Subject age at baseline ranged from 59.51 to 89.56 years (mean = 73.64, SD = 5.84). The mean age at baseline of men was 74.14 (6.25) years and of women was 73.18 (5.43) years, which were not significantly different (two-sample t-test: $t = 1.51$, $df = 338$, $P = .13$). The mean education level of the entire cohort was 16.5 (2.7) years. The male subjects had significantly more years of education than the female subjects (two-sample t-test: $t = 4.37$, $df = 338$, $P < .001$). The mean ICV in males was significantly greater than that of females (two-sample t-test: $t = 12.46$, $df = 336$, $P < .001$). 87 of the 340 subjects (25.6%) were *APOE* ϵ4 carriers. The proportion of *APOE* ϵ4 carriers in men (23.5%) was not significantly different from that in women (27.5%) ($\chi^2 = .74$, $df = 1$, $p = .39$) (Table 2).

From the total of 4239 scans, 1737 (41%) were acquired using 1.5 T

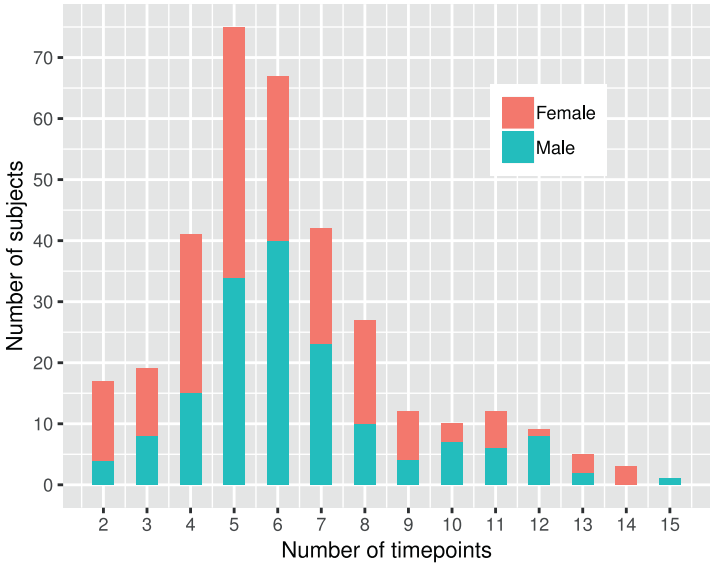

Fig. 4. Histogram of the number of subjects by number of timepoints. The histogram shows, for example, 75 subjects had 5 scanning sessions (timepoints) each.

and 2502 (59%) were acquired using 3 T MRI scanners (Table 2).[2] In women, 61.8% of scans were acquired at 3 T. The proportion of 3 T scans in men (56.2%) was significantly lower ($\chi^2 = 14$, $df = 1$, $P < .001$). Conversely, a significantly higher proportion of scans in men were at 1.5 T (43.8%) when compared to women (38.2%).

The histogram of the number of timepoints (ADNI scanning visits) by number of subjects is shown in Figure 4. The number of visits ranged from 2 to 15 with a median of 6 timepoints per subject. Most subjects (75) had 5 scanning visits (mode of the histogram). At each visit, subjects normally had two 3D T_1-weighted MRI scans. The number of scans per subject ranged from 3 to 35 with a median of 11.5. The duration of observation per subject ranged from 2 to 13.53 years with a mean of 4.95 (2.66) years.

3.2. Model parameter estimates

Table 3 shows the estimated fixed effect parameters in model (1). The random effects standard deviations for this model were estimated to be: $\hat{\sigma}_b = .054$, $\hat{\sigma}_a = .0046$ yr^{-1}, and $\hat{\sigma}_e = .02$. This information is sufficient to establish normative values of HPF. Sections 3.3-3.7 present results on the effects of specific factors and variables on the expected HPF values.

Table 4 shows the estimated fixed effect parameters in model (2). The random effects standard deviations for this model were estimated to be: $\hat{\sigma}_b = 2.71$, $\hat{\sigma}_a = .29$ yr^{-1}, and $\hat{\sigma}_e = 2.73$. Sections 3.8 and 3.9 present results on the effects of specific factors and variables on the expected ADAS-Cog-13 scores.

3.3. Effects of sex and brain hemisphere on HPF

The estimated marginal means (95% confidence interval) (CI) of HPF for median baseline age (73 years), median education level (16 years), mean ICV (1511 cm^3), *APOE* ϵ4 non-carriers, scanned at 3 T are shown in Figure 5. After correcting for all other variables, HPF was not significantly different between male and female subjects (β_1, Table 3, $P = .492$). However, the HPF on the right hemisphere was significantly larger than on the left (β_2, Table 3, $P < .001$); and this right > left asymmetry was significantly more pronounced in men compared to women (β_3, Table 3, $P < .001$).

[2] MPRAGEMETA.csv indicates 53 scans as having been acquired at a magnetic field strength of 2.9 T! We counted these as 3 T.

Table 3
Estimated fixed effects parameters for HPF in model (1)

Parameter	Estimate	Std. Error	P-value
β_0 (intercept)	8.588×10^{-1}	5.1×10^{-3}	< .001
β_1 (male)	-5.147×10^{-3}	7.5×10^{-3}	.492
β_2 (right)	8.092×10^{-3}	6.1×10^{-4}	< .001
β_3 (male and right)	3.008×10^{-3}	8.7×10^{-4}	< .001
β_4 (1.5 T)	-7.707×10^{-3}	9.3×10^{-4}	< .001
β_5 (education)	-3.232×10^{-3}	1.2×10^{-3}	.007
β_6 (*APOE*ϵ4 +)	-1.295×10^{-2}	7.1×10^{-3}	.069
β_7 (age)	-7.201×10^{-3}	3.8×10^{-4}	< .001
β_8 (age × *APOE*ϵ4 +)	-1.942×10^{-3}	7.0×10^{-4}	.006
β_9 (age-squared)	-1.656×10^{-4}	2.1×10^{-5}	< .001
β_{10} (ICV)	-9.166×10^{-3}	3.8×10^{-3}	.015

Table 4
Estimated fixed effects parameters for ADAS-Cog-13 in model (2)

Parameter	Estimate	Std. Error	P-value
β_0 (intercept)	6.83	.28	< .001
β_1 (*APOE*ϵ4 +)	.59	.42	.162
β_2 (male)	1.56	.37	< .001
β_3 (HPF)	−.085	.027	.002
β_4 (education)	−.28	.07	< .001
β_5 (age)	.13	.04	.003
β_6 (age × *APOE*ϵ4 +)	.11	.07	.126
β_7 (age-squared)	.01	.0028	< .001

3.4. Scanner bias in HPF

We found a scanner effect whereby the estimated HPF using 1.5 T scanners was slightly but significantly lower than the estimated HPF using 3 T scanners (β_4, Table 3, $P < .001$). The difference as a percentage of mean HPF was -.9 (-1.1, -.7) (%).

3.5. Effect of education on HPF

There was a negative association between years of education and HPF (β_5, Table 3, $P = .007$). As a percentage of mean HPF, the rate of change with education level was -.38 (-.65, -.10) (%/education yr).

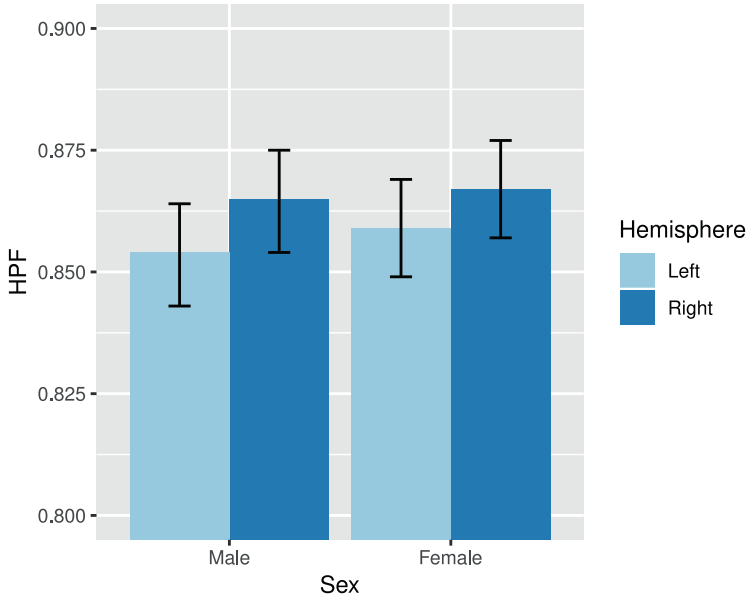

Fig. 5. Estimated marginal means for men and women on the left and right hemispheres. The error bars represent the 95% confidence intervals.

3.6. Effects of age and APOE genotype on HPF

There was a trend towards a reduction in HPF in *APOE* ϵ4 carriers (i.e., subjects with 1 or 2 copies of the *APOE* ϵ4 allele) relative to non-carriers (β_6, Table 3, $P = .069$). *APOE* genotype did significantly affect the rate of decline of HPF with age. As a percentage of mean HPF (.861), HPF in ϵ4 non-carriers declined at a rate of -.84 (-.92, -.75) (%/yr) (β_7, Table 3, $P < .001$). The decline rate in ϵ4 carriers was significantly faster (β_8, Table 3, $P = .006$), amounting to -1.06 (-1.20, -.92) (%/yr).

There was also strong evidence that HPF declined quadratically with age (β_9, Table 3, $P < .001$). The acceleration of HPF decline ($2\beta_9$) as a percentage of mean HPF was estimated to be -.04 (-.05, -.03) (%/yr^2).

3.7. Effect of ICV on HPF

Controlling for all other variables, there was a signifincant negative association between ICV and HPF (β_{10}, Table 3, $P = .015$). For every one SD (154.5 cm^3) increase in ICV the HPF declined by -1.06 (-1.92, -0.21) (%/SD).

3.8. Effects of sex, education, APOE genotype, and age on ADAS-Cog-13

The mean ADAS-Cog-13 score was estimated to be 6.83 (6.28, 7.37) for females (β_0, Table 4) and 8.39 (7.80, 8.97) for males ($\beta_0 + \beta_2$, Table 4). Males performed significantly worse than females ($P < .001$).

The ADAS-Cog-13 scores improved (decreased) with increasing education level at a rate of -.28 (-.42, -.14) (pts/yr). This rate of improvement (β_4, Table 4) was statistically significant ($P < .001$).

The *APOE* ϵ4 carriers performed slightly worse than non-carriers (β_1, Table 4) and their cognitive ability declined slightly faster than non-carriers (β_6, Table 4); however, neither effect reached statistical significance ($P = .162$ and $P = .126$, respectively).

ADAS-Cog-13 scores worsened quadratically with age as indicated by significantly positive β_5 ($P = .003$) and β_7 ($P < .001$) coefficients in Table 4.

3.9. Effect of HPF on ADAS-Cog-13

After controlling for sex, education, *APOE* genotype, and age, there was a significant association between HPF and ADAS-Cog-13 (β_3, Table 4, $P = .002$). For every .01 unit increase in HPF the ADAS-Cog-13 score declined (improved) by -.085 (-.138, -.032) points.

4. Discussion

The hippocampal parenchymal fraction is a recently developed clinically viable neuroimaging biomarker of hippocampal degeneration (Ardekani et al., 2017; 2016; Bruno et al., 2016; Goff et al., 2018; Hakimi et al., 2019; Mubeen et al., 2017). It can be computed rapidly and robustly on raw structural MRI scans without a need for image preprocessing or operator expertise. The main objective of this paper was to establish the normative values of HPF and its rate of decline with age in cognitively normal individuals to enhance the potential of this measure both clinically, and as a research tool for developing therapeutic interventions. Our results show that factors such as age, sex, *APOE* genotype, ICV, and brain hemisphere significantly affect HPF values and therefore should be taken into account when evaluating HPF in individual cases. By and large, our findings are in concordance with the literature on HC volume measurements in normally aging individuals.

We found a right > left asymmetry in HPF (β_2, Table 3; Figure 5). This is in concordance with several previous studies that have also found that the right HC volume was larger than the left in normal aging, MCI and AD (Barnes et al., 2005; Maller et al., 2007; Shi et al., 2009; Wachinger et al., 2016; Ystad et al., 2009). In addition, we found that this asymmetry is slightly more pronounced in males (β_3, Table 3; Figure 5) which replicates the results that we recently found in a different cohort (OASIS1) (Ardekani et al., 2019) as well as those reported by Lucarelli et al. (2013).

The HPF declined with age quadratically. The decline rate of HPF with age was estimated to be -.84 (-.92, -.75) (%/yr) for an individual at median age, and to increase by -.04 (%/yr) per year thereafter. The normal age-related decline in HC volume is a common finding (Armstrong et al., 2019; Cohen et al., 2001; Cover et al., 2016; Knoops et al., 2012; Ystad et al., 2009). In addition, we found that the rate of decline in *APOE* ϵ4 carriers, -1.06 (-1.20, -.92) (%/yr), was significantly faster than non-carriers. This is also corroborated by a number of previously published works (Armstrong et al., 2019; Cohen et al., 2001; Fleisher et al., 2005; Spampinato et al., 2016).

An initially surprising finding was a negative linear association between HPF and years of education (β_5, Table 3) after correcting for all other variables (section 3.5). On average, HPF declined by -.38 (-.65,

-.10) %/(education yr). Since in this cohort, men were significantly more educated than women (Table 2), we stratified the cohort by sex and repeated the linear mixed effects model analysis for men and women separately. We still observed the negative association between education and HPF. At the same time, the ADAS-Cog-13 scores improved (decreased) significantly with an increasing education level ($P < .001$) (section 3.8) after controlling for all other variables. The ADAS-Cog-13 scores declined (ability improved) by an average of -.28 (-.42, -.14) pts/(education yr). We hypothesize that these findings may be due to *cognitive reserve* (Stern, 2012), whereby people with higher levels of education can tolerate more HC atrophy and still maintain a level of function that allows them to be classified as cognitively normal throughout the study period.

The HPF was found to decline with increasing ICV (β_{10}, Table 3), reducing by -1.06% (-1.92%, -0.21%) for every SD units increase in ICV (section 3.7). This result is in agreement with our previous finding on an independent cohort (Ardekani et al., 2019). It should be noted that in this respect HPF is different from HC volume, since the latter has been consistently found to *increase* in proportion to ICV (Bosco et al., 2017; Fleisher et al., 2005; Ystad et al., 2009). We attribute the negative association between HPF and ICV to the fact that HPF in some sense measures the compactness of brain tissue within the cranium. Therefore, it is conceivable that a smaller ICV would result in more compact brain tissue compartments and, therefore, higher HPF. Based on our experience with analysing MRI scans for both HPF and HC volume, we hypothesize that the latter depends more strongly on ICV than the former, since HPF is a normalized measure. This hypothesis remains to be formally tested.

The finding that ADAS-Cog-13 scores improved with education level (section 3.8) is also consistent with multiple previously published research articles that show a positive association between performance on neuropsychological tests and education level in normal elderly subjects (Ganguli et al., 1991; 2010; van Hooren et al., 2007; Melikyan et al., 2019; Snitz et al., 2009).

The female subjects performed significantly better than the male subjects on the ADAS-Cog-13 neurocognitive test battery ($P < .001$) by about 1.5 points (section 3.8). This is consistent with multiple previously published research papers showing that normal elderly women perform better than their male counterparts, particularly in neuropsychiatric tests involving verbal memory and recall (Collie et al., 1999; Gale et al., 2007; Ganguli et al., 1991; van Hooren et al., 2007; Munro et al., 2012; Ystad et al., 2009). Interestingly, in patients with early stage dementia this trend reverses, that is, cognitive impairment in female patients appears to progress faster than in males (Lin et al., 2015; Sohn et al., 2018) and the advantage in CN females (relative to males) may disappear in MCI (Gale et al., 2016) and even reverse in AD. According to Chapman et al. (2011): “women have farther to fall”. This suggests the gap between CN and AD groups is wider in women than men in neurocognitive scores. Therefore, when these features are used for classification, machine learning algorithms perform more accurately in detecting AD in women that in men (Ardekani et al., 2017; Mubeen et al., 2017).

We also found that ADAS-Cog-13 performance declined (scores increased) quadratically with age (section 3.8). This is in agreement with numerous other papers that have also noted a decline in cognitive ability with age (Collie et al., 1999; Gale et al., 2007; Ganguli et al., 1991; van Hooren et al., 2007; Ystad et al., 2009).

We did not find a statistically significant difference between ADAS-Cog-13 of $\epsilon 4$ carriers and non-carriers. Nor did we find a statistically significant difference between their decline rates in performance. Some recent studies have found that, in non-demented older adults, $\epsilon 4$-carriers demonstrate a more rapid decline in executive function and memory (Chapman et al., 2018; Reas et al., 2019). On the other hand, a meta-analysis of the effects of *APOE* $\epsilon 4$ in mid-adulthood (defined as a mean sample age between 35 and 60 years) found the average effect size of $\epsilon 4$ to be non-significant across cognitive domains (Lancaster et al., 2017). The subjects in this longitudinal study had a median of three ADAS-Cog-13 assessments each. Therefore, it is possible that the effects of aging on the ADAS-Cog-13 score are somewhat attenuated due to a practice effect.

After adjusting for sex, education, age, and *APOE* genotype, we found that HPF was significantly associated with ADAS-Cog-13 scores (section 3.9). For every .01 unit increase in HPF, the ADAS-Cog-13 score declined by -.085 (-.138, -.032) points. Conversely, HC atrophy was associated with a decline in cognitive ability. This finding is clinically important because evaluation of HPF by MRI offers a neurobiological substrate for cognitive decline. Patients with SMC accompanied with quantifiably low HPF may be at a higher risk of incipient dementia. It has been shown that augmenting clinical and cognitive measures with MRI-based HC volume measurements increases the diagnostic confidence of AD pathology (Bosco et al., 2017).

This study has a number of limitations. In 82 images (out of 4239) or 1.9%, the KAIBA software failed to detect the MSP and/or the AC/PC automatically. For these images this information had to be supplied manually in order to measure the HPF. Future research is required to reduce this failure rate. As with any other analysis using linear mixed effects models, there is a risk that the model assumptions of homoscedasticity, normalities of random effects and residuals, and linear associations between independent and predictor variables are not satisfied. In this work, we qualitatively checked for model assumptions using Q-Q plots and by plotting residuals versus HPF fits and ensured that these assumptions are reasonably valid. In addition, the significance levels of our findings were generally quite high and it is unlikely that minor violations of the model assumptions would change our conclusions. There are likely other factors such as socioeconomic status, MRI pulse-sequences (e.g., accelerated vs fully sampled), handedness, etc. that could systematically affect HPF but were not considered in this study. Due to the large number of scans (4239), we did not include a direct comparison between HPF and automaticed HC volumetry (e.g., FreeSurfer). This remains for a future study. In this study, we investigated the relationship between HPF on ADAS-Cog-13 in CN. The ADAS-Cog-13 was developed to measure behavioral/cognitive deficit severity in symptomatic AD patients. Reviews of its use in a number of MCI and CN cohorts demonstrate ceiling effects in the majority of tasks, with most errors in word recall and word recognition (Kueper et al., 2018). Separating cognitive performance by task could provide insight to some of the significant effectors on ADAS-Cog-13 scores.

5. Conclusions

The HPF is a promising neuroimaging biomarker of HC atrophy. In this paper, we established normative values of HPF with respect to sex, age, *APOE* genotype, scanner field strength, brain hemisphere, ICV, and education level. We found that (1) HPF decreased with increasing ICV, (2) HPF was higher on the right hemisphere than left, (3) the right > left asymmetry was slightly more pronounced in men, (4) HPF decreases quadratically with age, (5) the rate of HPF decline with age was faster in *APOE* $\epsilon 4$ carriers than non-carriers, and (6) after controlling for age, sex, education and $\epsilon 4$ status, HPF was significantly associated with cognitive ability. The results were in close agreement with previously published research based on HC volume. When evaluating HPF on single individuals, these factors need to be considered. HPF has potential as a biomarker in research studies and clinical diagnosis of AD.

Disclosure Statement: No conflicts of interest exist

Aknowledgements

Data collection and sharing for this project was funded by the Alzheimer’s Disease Neuroimaging Initiative (ADNI) (National Institutes of Health Grant U01 AG024904) and DOD ADNI (Department of Defense award number W81XWH-12-2-0012). ADNI is funded by the

National Institute on Aging, the National Institute of Biomedical Imaging and Bioengineering, and through generous contributions from the following: AbbVie, Alzheimer's Association; Alzheimer's Drug Discovery Foundation; Araclon Biotech; BioClinica, Inc.; Biogen; Bristol-Myers Squibb Company; CereSpir, Inc.; Cogstate; Eisai Inc.; Elan Pharmaceuticals, Inc.; Eli Lilly and Company; EuroImmun; F. Hoffmann-La Roche Ltd and its affiliated company Genentech, Inc.; Fujirebio; GE Healthcare; IXICO Ltd.; Janssen Alzheimer Immunotherapy Research & Development, LLC.; Johnson & Johnson Pharmaceutical Research & Development LLC.; Lumosity; Lundbeck; Merck & Co., Inc.; Meso Scale Diagnostics, LLC.; NeuroRx Research; Neurotrack Technologies; Novartis Pharmaceuticals Corporation; Pfizer Inc.; Piramal Imaging; Servier; Takeda Pharmaceutical Company; and Transition Therapeutics. The Canadian Institutes of Health Research is providing funds to support ADNI clinical sites in Canada. Private sector contributions are facilitated by the Foundation for the National Institutes of Health (www.fnih.org). The grantee organization is the Northern California Institute for Research and Education, and the study is coordinated by the Alzheimer's Therapeutic Research Institute at the University of Southern California. ADNI data are disseminated by the Laboratory for Neuro Imaging at the University of Southern California.

References

Ardekani, B.A., Bachman, A.H., 2009. Model-based automatic detection of the anterior and posterior commissures on MRI scans. Neuroimage 46 (3), 677–682.
Ardekani, B.A., Bermudez, E., Mubeen, A.M., Bachman, A.H., 2017. Prediction of Incipient Alzheimer's Disease Dementia in Patients with Mild Cognitive Impairment. J. Alzheimers Dis. 55 (1), 269–281.
Ardekani, B.A., Convit, A., Bachman, A.H., 2016. Analysis of the MIRIAD Data Shows Sex Differences in Hippocampal Atrophy Progression. J. Alzheimers Dis. 50 (3), 847–857.
Ardekani, B.A., Hadid, S.A., Blessing, E., Bachman, A.H., 2019. Sexual Dimorphism and Hemispheric Asymmetry of Hippocampal Volumetric Integrity in Normal Aging and Alzheimer Disease. AJNR Am J Neuroradiol 40 (2), 276–282.
Ardekani, B.A., Kershaw, J., Braun, M., Kanno, I., 1997. Automatic detection of the mid-sagittal plane in 3-D brain images. IEEE Trans Med Imaging 16 (6), 947–952.
Armstrong, N.M., An, Y., Beason-Held, L., Doshi, J., Erus, G., Ferrucci, L., Davatzikos, C., Resnick, S.M., 2019. Sex differences in brain aging and predictors of neurodegeneration in cognitively healthy older adults. Neurobiol. Aging 81, 146–156.
Barnes, J., Scahill, R.I., Schott, J.M., Frost, C., Rossor, M.N., Fox, N.C., 2005. Does Alzheimer's disease affect hippocampal asymmetry? Evidence from a cross-sectional and longitudinal volumetric MRI study. Dement Geriatr Cogn Disord 19 (5-6), 338–344.
Bates, D., Mächler, M., Bolker, B., Walker, S., 2015. Fitting linear mixed-effects models using lme4. J. Stat. Software 67 (1), 1–48.
Bosco, P., Redolfi, A., Bocchetta, M., Ferrari, C., Mega, A., Galluzzi, S., Austin, M., Chincarini, A., Collins, D.L., Duchesne, S., Marechal, B., Roche, A., Sensi, F., Wolz, R., Alegret, M., Assal, F., Balasa, M., Bastin, C., Bougea, A., Emek-Sava?, D.D., Engelborghs, S., Grimmer, T., Grosu, G., Kramberger, M.G., Lawlor, B., Mandic Stojmenovic, G., Marinescu, M., Mecocci, P., Molinuevo, J.L., Morais, R., Niemantsverdriet, E., Nobili, F., Ntovas, K., O'Dwyer, S., Paraskevas, G.P., Pelini, L., Picco, A., Salmon, E., Santana, I., Sotolongo-Grau, O., Spiru, L., Stefanova, E., Popovic, K.S., Tsolaki, M., Yener, G.G., Zekry, D., Frisoni, G.B., 2017. The impact of automated hippocampal volumetry on diagnostic confidence in patients with suspected Alzheimer's disease: A European Alzheimer's Disease Consortium study. Alzheimers Dement 13 (9), 1013–1023.
Bruno, D., Ciarleglio, A., Grothe, M.J., Nierenberg, J., Bachman, A.H., Teipel, S.J., Petkova, E., Ardekani, B.A., Pomara, N., 2016. Hippocampal volume and integrity as predictors of cognitive decline in intact elderly. Neuroreport 27 (11), 869–873.
Cardoso, M.J., Leung, K., Modat, M., Keihaninejad, S., Cash, D., Barnes, J., Fox, N.C., Ourselin, S., 2013. STEPS: Similarity and Truth Estimation for Propagated Segmentations and its application to hippocampal segmentation and brain parcelation. Med Image Anal 17 (6), 671–684.
Chapman, B.P., Benedict, R.H.B., Lin, F., Roy, S., Porteinsson, A., Szigeti, K., Federoff, H., Mapstone, M., 2018. Apolipoprotein E genotype impact on memory and attention in older persons: the moderating role of personality phenotype. Int J Geriatr Psychiatry 33 (2), 332–339.
Chapman, R.M., Mapstone, M., Gardner, M.N., Sandoval, T.C., McCrary, J.W., Guillily, M.D., Reilly, L.A., DeGrush, E., 2011. Women have farther to fall: gender differences between normal elderly and Alzheimer's disease in verbal memory engender better detection of Alzheimer's disease in women. J Int Neuropsychol Soc 17 (4), 654–662.
Chupin, M., Hammers, A., Liu, R.S., Colliot, O., Burdett, J., Bardinet, E., Duncan, J.S., Garnero, L., Lemieux, L., 2009. Automatic segmentation of the hippocampus and the amygdala driven by hybrid constraints: method and validation. Neuroimage 46 (3), 749–761.
Cohen, R.M., Small, C., Lalonde, F., Friz, J., Sunderland, T., 2001. Effect of apolipoprotein E genotype on hippocampal volume loss in aging healthy women. Neurology 57 (12), 2223–2228.
Collie, A., Shafiq-Antonacci, R., Maruff, P., Tyler, P., Currie, J., 1999. Norms and the effects of demographic variables on a neuropsychological battery for use in healthy ageing Australian populations. Aust N Z J Psychiatry 33 (4), 568–575.
Collins, D.L., Pruessner, J.C., 2010. Towards accurate, automatic segmentation of the hippocampus and amygdala from MRI by augmenting ANIMAL with a template library and label fusion. Neuroimage 52 (4), 1355–1366.
Convit, A., De Leon, M.J., Tarshish, C., De Santi, S., Tsui, W., Rusinek, H., George, A., 1997. Specific hippocampal volume reductions in individuals at risk for Alzheimer's disease. Neurobiol. Aging 18 (2), 131–138.
Coupe, P., Manjon, J.V., Fonov, V., Pruessner, J., Robles, M., Collins, D.L., 2010. Nonlocal patch-based label fusion for hippocampus segmentation. Med Image Comput Comput Assist Interv 13 (Pt 3), 129–136.
Coupe, P., Manjon, J.V., Fonov, V., Pruessner, J., Robles, M., Collins, D.L., 2011. Patch-based segmentation using expert priors: application to hippocampus and ventricle segmentation. Neuroimage 54 (2), 940–954.
Cover, K.S., van Schijndel, R.A., Versteeg, A., Leung, K.K., Mulder, E.R., Jong, R.A., Visser, P.J., Redolfi, A., Revillard, J., Grenier, B., Manset, D., Damangir, S., Bosco, P., Vrenken, H., van Dijk, B.W., Frisoni, G.B., Barkhof, F., 2016. Reproducibility of hippocampal atrophy rates measured with manual, FreeSurfer, AdaBoost, FSL/FIRST and the MAPS-HBSI methods in Alzheimer's disease. Psychiatry Res Neuroimaging 252, 26–35.
Dill, V., Franco, A.R., Pinho, M.S., 2015. Automated methods for hippocampus segmentation: the evolution and a review of the state of the art. Neuroinformatics 13 (2), 133–150.
Fischl, B., Salat, D.H., Busa, E., Albert, M., Dieterich, M., Haselgrove, C., van der Kouwe, A., Killiany, R., Kennedy, D., Klaveness, S., Montillo, A., Makris, N., Rosen, B., Dale, A.M., 2002. Whole brain segmentation: automated labeling of neuroanatomical structures in the human brain. Neuron 33 (3), 341–355.
Fleisher, A., Grundman, M., Jack, C.R., Petersen, R.C., Taylor, C., Kim, H.T., Schiller, D.H., Bagwell, V., Sencakova, D., Weiner, M.F., DeCarli, C., DeKosky, S.T., van Dyck, C.H., Thal, L.J., 2005. Sex, apolipoprotein E epsilon 4 status, and hippocampal volume in mild cognitive impairment. Arch. Neurol. 62 (6), 953–957.
Gale, S.D., Baxter, L., Connor, D.J., Herring, A., Comer, J., 2007. Sex differences on the Rey Auditory Verbal Learning Test and the Brief Visuospatial Memory Test-Revised in the elderly: normative data in 172 participants. J Clin Exp Neuropsychol 29 (5), 561–567.
Gale, S.D., Baxter, L., Thompson, J., 2016. Greater memory impairment in dementing females than males relative to sex-matched healthy controls. J Clin Exp Neuropsychol 38 (5), 527–533.
Ganguli, M., Ratcliff, G., Huff, F.J., Belle, S., Kancel, M.J., Fischer, L., Seaberg, E.C., Kuller, L.H., 1991. Effects of age, gender, and education on cognitive tests in a rural elderly community sample: norms from the Monongahela Valley Independent Elders Survey. Neuroepidemiology 10 (1), 42–52.
Ganguli, M., Snitz, B.E., Lee, C.W., Vanderbilt, J., Saxton, J.A., Chang, C.C., 2010. Age and education effects and norms on a cognitive test battery from a population-based cohort: the Monongahela-Youghiogheny Healthy Aging Team. Aging Ment Health 14 (1), 100–107.
Goff, D.C., Zeng, B., Ardekani, B.A., Diminich, E.D., Tang, Y., Fan, X., Galatzer-Levy, I., Li, C., Troxel, A.B., Wang, J., 2018. Association of Hippocampal Atrophy With Duration of Untreated Psychosis and Molecular Biomarkers During Initial Antipsychotic Treatment of First-Episode Psychosis. JAMA Psychiatry 75 (4), 370–378.
Hakimi, M., Ardekani, B.A., Pressl, C., Blackmon, K., Thesen, T., Devinsky, O., Kuzniecky, R.I., Pardoe, H.R., 2019. Hippocampal volumetric integrity in mesial temporal lobe epilepsy: A fast novel method for analysis of structural MRI. Epilepsy Res. 154, 157–162.
Heister, D., Brewer, J.B., Magda, S., Blennow, K., McEvoy, L.K., Jagust, W., Trojanowki, J., Toga, A.W., Beckett, L., Green, R.C., Gamst, A., Saykin, A.J., Morris, J., Potter, W.Z., Montine, T., Thomas, R.G., Donohue, M., Walter, S., Dale, A., Bernstein, M., Felmlee, J., Fox, N., Thompson, P., Alexander, G., DeCarli, C., Bandy, D., Koeppe, R.A., Foster, N., Reiman, E.M., Chen, K., Mathis, C., Cairns, N.J., Taylor-Reinwald, L., Shaw, L., Lee, V.M., Korecka, M., Crawford, K., Neu, S., Harvey, D., Kornak, J., Saykin, A.J., Foroud, T.M., Potkin, S., Shen, L., Kachaturian, Z., Frank, R., Snyder, P.J., Molchan, S., Kaye, J., Dolen, S., Quinn, J., Schneider, L., Pawluczyk, S., Spann, B.M., Brewer, J., Vanderswag, H., Heidebrink, J.L., Lord, J.L., Johnson, K., Doody, R.S., Villanueva-Meyer, J., Chowdhury, M., Stern, Y., Honig, L.S., Bell, K.L., Mintun, M.A., Schneider, S., Marson, D., Griffith, R., Clark, D., Grossman, H., Tang, C., Marzloff, G., deToledo Morrell, L., Shah, R.C., Duara, R., Varon, D., Roberts, P., Albert, M.S., Kozauer, N., Zerrate, M., Rusinek, H., de Leon, M.J., De Santi, S.M., Doraiswamy, P.M., Petrella, J.R., Aiello, M., Arnold, S., Karlawish, J.H., Wolk, D., Smith, C.D., Given, C.A., Hardy, P., Lopez, O.L., Oakley, M., Simpson, D.M., Ismail, M.S., Brand, C., Richard, J., Mulnard, R.A., Thai, G., McAdams-Ortiz, C., Diaz-Arrastia, R., Martin-Cook, K., DeVous, M., Levey, A.I., Lah, J.J., Cellar, J.S., Burns, J.M., Anderson, H.S., Laubinger, M.M., Apostolova, L., Silverman, D.H., Lu, P.H., Graff-Radford, N.R., Parfitt, F., Johnson, H., Farlow, M., Herring, S., Hake, A.M., van Dyck, C.H., MacAvoy, M.G., Benincasa, A.L., Chertkow, H., Bergman, H., Hosein, C., Black, S., Stefanovic, B., Caldwell, C., Hsiung, G.Y., Feldman, H., Assaly, M., Kertesz, A., Rogers, J., Trost, D., Bernick, C., Munic, D., Wu, C.K., Johnson, N., Mesulam, M., Sadowsky, C., Martinez, W., Villena, T., Turner, R.S., Johnson, K., Reynolds, B., Sperling, R.A., Rentz, D.M., Johnson, K.A., Rosen, A., Tinklenberg, J., Ashford, W., Sabbagh, M., Connor, D., Jacobson, S., Killiany, R., Norbash, A., Nair, A., Obisesan, T.O., Jayam-Trouth, A., Wang, P., Lerner, A., Hudson, L., Ogrocki, P., DeCarli, C., Fletcher, E., Carmichael, O., Kittur, S., Borrie, M., Lee, T.Y., Bartha, R., Johnson, S., Asthana, S., Carlsson, C.M., Potkin, S.G., Preda, A., Nguyen, D., Tariot, P., Fleisher, A., Reeder, S., Bates, V., Capote, H., Rainka, M., Hendin, B.A., Scharre, D.W., Kataki, M., Zimmerman, E.A., Celmins, D., Brown, A.D., Pearlson, G., Blank, K., Anderson, K., Saykin, A.J., Santulli, R.B., Englert, J., Williamson, J.D., Sink, K.M., Watkins, F., Ott,

B.R., Stopa, E., Tremont, G., Salloway, S., Malloy, P., Correia, S., Rosen, H.J., Miller, B.L., Mintzer, J., Flynn Longmire, C., Spicer, K., 2011. Predicting MCI outcome with clinically available MRI and CSF biomarkers. Neurology 77 (17), 1619–1628.

van Hooren, S.A., Valentijn, A.M., Bosma, H., Ponds, R.W., van Boxtel, M.P., Jolles, J., 2007. Cognitive functioning in healthy older adults aged 64-81: a cohort study into the effects of age, sex, and education. Neuropsychol Dev Cogn B Aging Neuropsychol Cogn 14 (1), 40–54.

Hu, S., Coupe, P., Pruessner, J.C., Collins, D.L., 2011. Appearance-based modeling for segmentation of hippocampus and amygdala using multi-contrast MR imaging. Neuroimage 58 (2), 549–559.

Jack, C.R., Barnes, J., Bernstein, M.A., Borowski, B.J., Brewer, J., Clegg, S., Dale, A.M., Carmichael, O., Ching, C., DeCarli, C., Desikan, R.S., Fennema-Notestine, C., Fjell, A.M., Fletcher, E., Fox, N.C., Gunter, J., Gutman, B.A., Holland, D., Hua, X., Insel, P., Kantarci, K., Killiany, R.J., Krueger, G., Leung, K.K., Mackin, S., Maillard, P., Malone, I.B., Mattsson, N., McEvoy, L., Modat, M., Mueller, S., Nosheny, R., Ourselin, S., Schuff, N., Senjem, M.L., Simonson, A., Thompson, P.M., Rettmann, D., Vemuri, P., Walhovd, K., Zhao, Y., Zuk, S., Weiner, M., 2015. Magnetic resonance imaging in Alzheimer's Disease Neuroimaging Initiative 2. Alzheimers Dement 11 (7), 740–756.

Jack, C.R., Bernstein, M.A., Borowski, B.J., Gunter, J.L., Fox, N.C., Thompson, P.M., Schuff, N., Krueger, G., Killiany, R.J., Decarli, C.S., Dale, A.M., Carmichael, O.W., Tosun, D., Weiner, M.W., 2010. Update on the magnetic resonance imaging core of the Alzheimer's disease neuroimaging initiative. Alzheimers Dement 6 (3), 212–220.

Jack, C.R., Bernstein, M.A., Fox, N.C., Thompson, P., Alexander, G., Harvey, D., Borowski, B., Britson, P.J., L Whitwell, J., Ward, C., Dale, A.M., Felmlee, J.P., Gunter, J.L., Hill, D.L., Killiany, R., Schuff, N., Fox-Bosetti, S., Lin, C., Studholme, C., DeCarli, C.S., Krueger, G., Ward, H.A., Metzger, G.J., Scott, K.T., Mallozzi, R., Blezek, D., Levy, J., Debbins, J.P., Fleisher, A.S., Albert, M., Green, R., Bartzokis, G., Glover, G., Mugler, J., Weiner, M.W., 2008. The Alzheimer's Disease Neuroimaging Initiative (ADNI): MRI methods. J Magn Reson Imaging 27 (4), 685–691.

Jack, C.R., Petersen, R.C., Xu, Y., O'Brien, P.C., Smith, G.E., Ivnik, R.J., Tangalos, E.G., Kokmen, E., 1998. Rate of medial temporal lobe atrophy in typical aging and Alzheimer's disease. Neurology 51 (4), 993–999.

Jack, C.R., Petersen, R.C., Xu, Y.C., O'Brien, P.C., Smith, G.E., Ivnik, R.J., Boeve, B.F., Waring, S.C., Tangalos, E.G., Kokmen, E., 1999. Prediction of AD with MRI-based hippocampal volume in mild cognitive impairment. Neurology 52 (7), 1397–1403.

Knoops, A.J., Gerritsen, L., van der Graaf, Y., Mali, W.P., Geerlings, M.I., 2012. Loss of entorhinal cortex and hippocampal volumes compared to whole brain volume in normal aging: the SMART-Medea study. Psychiatry Res 203 (1), 31–37.

Konrad, C., Ukas, T., Nebel, C., Arolt, V., Toga, A.W., Narr, K.L., 2009. Defining the human hippocampus in cerebral magnetic resonance images–an overview of current segmentation protocols. Neuroimage 47 (4), 1185–1195.

Kueper, J.K., Speechley, M., Montero-Odasso, M., 2018. The Alzheimer's Disease Assessment Scale-Cognitive Subscale (ADAS-Cog): Modifications and Responsiveness in Pre-Dementia Populations. A Narrative Review. J. Alzheimers Dis. 63 (2), 423–444.

Lancaster, C., Tabet, N., Rusted, J., 2017. The Elusive Nature of APOE e4 in Mid-adulthood: Understanding the Cognitive Profile. J Int Neuropsychol Soc 23 (3), 239–253.

Lee, S., Lee, H., Kim, K.W., 2019. Magnetic resonance imaging texture predicts progression to dementia due to Alzheimer disease earlier than hippocampal volume. J Psychiatry Neurosci 44 (5), 1–8.

de Leon, M.J., Golomb, J., George, A.E., Convit, A., Tarshish, C.Y., McRae, T., De Santi, S., Smith, G., Ferris, S.H., Noz, M., 1993. The radiologic prediction of Alzheimer disease: the atrophic hippocampal formation. AJNR Am J Neuroradiol 14 (4), 897–906.

Lin, K.A., Choudhury, K.R., Rathakrishnan, B.G., Marks, D.M., Petrella, J.R., Doraiswamy, P.M., 2015. Marked gender differences in progression of mild cognitive impairment over 8 years. Alzheimers Dement (N Y) 1 (2), 103–110.

Lucarelli, R.T., Peshock, R.M., McColl, R., Hulsey, K., Ayers, C., Whittemore, A.R., King, K.S., 2013. MR imaging of hippocampal asymmetry at 3T in a multiethnic, population-based sample: results from the Dallas Heart Study. AJNR Am J Neuroradiol 34 (4), 752–757.

Maller, J.J., Anstey, K.J., Reglade-Meslin, C., Christensen, H., Wen, W., Sachdev, P., 2007. Hippocampus and amygdala volumes in a random community-based sample of 60-64 year olds and their relationship to cognition. Psychiatry Res 156 (3), 185–197.

Maltbie, E., Bhatt, K., Paniagua, B., Smith, R.G., Graves, M.M., Mosconi, M.W., Peterson, S., White, S., Blocher, J., El-Sayed, M., Hazlett, H.C., Styner, M.A., 2012. Asymmetric bias in user guided segmentations of brain structures. Neuroimage 59 (2), 1315–1323.

Melikyan, Z.A., Corrada, M.M., Dick, M.B., Whittle, C., Paganini-Hill, A., Kawas, C.H., 2019. Neuropsychological Test Norms in Cognitively Intact Oldest-Old. J Int Neuropsychol Soc 25 (5), 530–545.

Mohs, R.C., Knopman, D., Petersen, R.C., Ferris, S.H., Ernesto, C., Grundman, M., Sano, M., Bieliauskas, L., Geldmacher, D., Clark, C., Thal, L.J., 1997. Development of cognitive instruments for use in clinical trials of antidementia drugs: additions to the Alzheimer's Disease Assessment Scale that broaden its scope. The Alzheimer's Disease Cooperative Study. Alzheimer Dis Assoc Disord 11 Suppl 2, 13–21.

Morra, J.H., Tu, Z., Apostolova, L.G., Green, A.E., Avedissian, C., Madsen, S.K., Parikshak, N., Hua, X., Toga, A.W., Jack, C.R., Weiner, M.W., Thompson, P.M., 2008. Validation of a fully automated 3D hippocampal segmentation method using subjects with Alzheimer's disease mild cognitive impairment, and elderly controls. Neuroimage 43 (1), 59–68.

Mubeen, A.M., Asaei, A., Bachman, A.H., Sidtis, J.J., Ardekani, B.A., 2017. A six-month longitudinal evaluation significantly improves accuracy of predicting incipient Alzheimer's disease in mild cognitive impairment. J Neuroradiol 44 (6), 381–387.

Mulder, E.R., de Jong, R.A., Knol, D.L., van Schijndel, R.A., Cover, K.S., Visser, P.J., Barkhof, F., Vrenken, H., 2014. Hippocampal volume change measurement: quantitative assessment of the reproducibility of expert manual outlining and the automated methods FreeSurfer and FIRST. Neuroimage 92, 169–181.

Munro, C.A., Winicki, J.M., Schretlen, D.J., Gower, E.W., Turano, K.A., Munoz, B., Keay, L., Bandeen-Roche, K., West, S.K., 2012. Sex differences in cognition in healthy elderly individuals. Neuropsychol Dev Cogn B Aging Neuropsychol Cogn 19 (6), 759–768.

Nestor, S.M., Gibson, E., Gao, F.Q., Kiss, A., Black, S.E., 2013. A direct morphometric comparison of five labeling protocols for multi-atlas driven automatic segmentation of the hippocampus in Alzheimer's disease. Neuroimage 66, 50–70.

R Core Team, 2018. R: A Language and Environment for Statistical Computing. R Foundation for Statistical Computing. Vienna, Austria.

Reas, E.T., Laughlin, G.A., Bergstrom, J., Kritz-Silverstein, D., Barrett-Connor, E., McEvoy, L.K., 2019. Effects of APOE on cognitive aging in community-dwelling older adults. Neuropsychology 33 (3), 406–416.

Rogers, B.P., Sheffield, J.M., Luksik, A.S., Heckers, S., 2012. Systematic Error in Hippocampal Volume Asymmetry Measurement is Minimal with a Manual Segmentation Protocol. Front Neurosci 6, 179.

Rosen, W.G., Mohs, R.C., Davis, K.L., 1984. A new rating scale for Alzheimer's disease. Am J Psychiatry 141 (11), 1356–1364.

Rusinek, H., De Santi, S., Frid, D., Tsui, W.H., Tarshish, C.Y., Convit, A., de Leon, M.J., 2003. Regional brain atrophy rate predicts future cognitive decline: 6-year longitudinal MR imaging study of normal aging. Radiology 229 (3), 691–696.

Shi, F., Liu, B., Zhou, Y., Yu, C., Jiang, T., 2009. Hippocampal volume and asymmetry in mild cognitive impairment and Alzheimer's disease: Meta-analyses of MRI studies. Hippocampus 19 (11), 1055–1064.

Snitz, B.E., Unverzagt, F.W., Chang, C.C., Bilt, J.V., Gao, S., Saxton, J., Hall, K.S., Ganguli, M., 2009. Effects of age, gender, education and race on two tests of language ability in community-based older adults. Int Psychogeriatr 21 (6), 1051–1062.

Sohn, D., Shpanskaya, K., Lucas, J.E., Petrella, J.R., Saykin, A.J., Tanzi, R.E., Samatova, N.F., Doraiswamy, P.M., 2018. Sex Differences in Cognitive Decline in Subjects with High Likelihood of Mild Cognitive Impairment due to Alzheimer's disease. Sci Rep 8 (1), 7490.

Spampinato, M.V., Langdon, B.R., Patrick, K.E., Parker, R.O., Collins, H., Pravata', E., 2016. Gender, apolipoprotein E genotype, and mesial temporal atrophy: 2-year follow-up in patients with stable mild cognitive impairment and with progression from mild cognitive impairment to Alzheimer's disease. Neuroradiology 58 (11), 1143–1151.

Stern, Y., 2012. Cognitive reserve in ageing and Alzheimer's disease. Lancet Neurol 11 (11), 1006–1012.

Suppa, P., Anker, U., Spies, L., Bopp, I., Ruegger-Frey, B., Klaghofer, R., Gocke, C., Hampel, H., Beck, S., Buchert, R., 2015. Fully automated atlas-based hippocampal volumetry for detection of Alzheimer's disease in a memory clinic setting. J. Alzheimers Dis. 44 (1), 183–193.

Wachinger, C., Salat, D.H., Weiner, M., Reuter, M., 2016. Whole-brain analysis reveals increased neuroanatomical asymmetries in dementia for hippocampus and amygdala. Brain 139 (Pt 12), 3253–3266.

Ystad, M.A., Lundervold, A.J., Wehling, E., Espeseth, T., Rootwelt, H., Westlye, L.T., Andersson, M., Adolfsdottir, S., Geitung, J.T., Fjell, A.M., Reinvang, I., Lundervold, A., 2009. Hippocampal volumes are important predictors for memory function in elderly women. BMC Med Imaging 9, 17.

Zhou, J., Rajapakse, J.C., 2005. Segmentation of subcortical brain structures using fuzzy templates. Neuroimage 28 (4), 915–924.